

Thermal Analysis of a Hypersonic Projectile using Semi-Empirical and FEA

A.A. Mabbett
 Naval Surface Warfare Center Dahlgren
 Dahlgren, VA

ABSTRACT

Hypersonic launch of a projectile in the low earth atmosphere presents several engineering obstacles. Structural survivability due to acceleration and thermal load management are significant difficulties. An extreme thermal environment on a relatively small object increases the complexity of the thermal protection system design. A baseline thermal model can assist with early designs and trade studies. This paper describes an initial thermal model created with the use of a semi-empirical aerodynamics code and finite element analysis (FEA). The thermal loads were determined from the semi-empirical aerodynamics code using standard heat transfer correlations as a function of the velocity and altitude as well as the physical design of the object. The heat loads were then applied as transient boundary conditions to a finite element model in order to capture the thermal time-history of the object.

INTRODUCTION

Over the last few decades, significant advances have occurred in support of electromagnetic launch (EML). The US Navy is currently considering an EM Railgun concept as a future long range naval weapons system. Preliminary studies have shown such a system will have the capability to launch a projectile upwards of 2.5 km/s over 200 nautical miles. Significant challenges exist in the design of a projectile system capable of withstanding this severe launch environment.¹

THERMAL ANALYSIS OF HYPERSONIC ROUND

Hypersonic Launch Conditions

The purpose of this analysis is to gain a better understanding of the thermal environment experienced of a hypersonically launched projectile at sea level as well as establish a baseline for design. For configuration ease a general cone shaped projectile was used with representative bulk mass fills [See below Figure 2]. One of the major engineering challenges associated with this project is the sea level hypersonic launch of a relatively small projectile less than 20 kg. [See Reference 1]

Configuration and Boundary Conditions

Initial estimates of the thermal profile were established in a first iteration via approximate hand calculation methods as well as a more refined yet still crude finite element model. The second iteration focused on refining the boundary conditions and begins incorporating internal masses. As a means for validating previous approximations, an empty airframe was analyzed initially; the addition of the tungsten nose fill and payload further enhanced the model detail.

With the use of Aeroprediction Code 2002 (AP02), a semi-empirical aerodynamics code, three degree of freedom trajectory models were obtained. Extracting the pertinent flight parameters and tabulating them versus time, a time-history profile was created for velocity and altitude. By feeding the velocity, altitude, and angle of attack into the aero-thermal module of AP02, a representative heat transfer coefficient and bulk temperature can be calculated for various points along the surface of the projectile as seen below⁴.

Stagnation Point

$$H = \frac{\dot{q}_w}{T_{aw} - T_w} \quad \text{Heat Transfer Coefficient}$$

$$T_{aw} = T_e + r_c(T_0 - T_e) \quad \text{Adiabatic Wall Temperature}$$

where:

Heat Transfer Rate

$$\dot{q}_w = 0.763 \text{Pr}^{-0.6} \sqrt{\rho_0 \mu_0} \sqrt{\frac{du_e}{dx}} (h_{aw} - h_w)$$

Pr = Prandtl Number ρ_0, μ_0 = stagnation density, viscosity

$$\sqrt{\frac{du_e}{dx}} = \frac{1}{r_N} \sqrt{\frac{2(p_0 - p_\infty)}{\rho_0}} \quad \text{Streamwise Vel. Gradient}$$

r_N = nose tip radius

p_0, p_∞ = stagnation and free stream pressure

$$h_{aw} = h_e + r_c(H_0 - h_e) \quad \text{Adiabatic Wall Enthalpy}$$

h_e = enthalpy at boundary layer edge

H_0 = Total enthalpy

$r_c = \text{Pr}^{1/2}$ (laminar) = $\text{Pr}^{1/3}$ (turbulent) Recovery Factor

T_e, T_0 = boundary layer edge and stagnation temperatures

Downstream Points

Laminar Heat Transfer Rate

$$\dot{q}_{w,l} = 0.332(\text{Pr}^*)^{-0.667} \frac{\rho^* V_b}{\sqrt{\frac{R_{Ne}^*}{N}}} (h_{aw} - h_w)$$

Turbulent Heat Transfer Rate

$$\dot{q}_{w,t} = 0.185(\text{Pr}^*)^{-0.667} \frac{\rho^* V_b}{\left(\ln\left(\frac{R_{Ne}^*}{N}\right)\right)^{2.584}} (h_{aw} - h_w)$$

where:

* conditions refer to values taken at the Eckert reference enthalpy,

h^* 4,5

$$h^* = 0.5(h_w + h_e) + 0.22(h_{aw} - h_e)$$

$$V_b = \sqrt{2(H_0 - h_e)}$$

$$R_{Ne} = \frac{\rho^* V_b s}{\mu} \quad s = \text{boundary layer running length}$$

$N = 3$ (laminar) = 2 (turbulent) Mangler transformation factor

Using these methodologies two cases were analyzed. The first case assumed a constant angle of attack (AOA) of zero degrees throughout the flight, whereas case two assumed a maximum constant ten degree AOA throughout the re-entry portion of the trajectory.

Finite Element Analysis

The analysis was performed initially on the airframe only (Figure 1) and then the tungsten nose-fill and payload was included (Figure 2). Each configuration was subjected to the same time-dependant boundary conditions (BC) attained from AP02. For the AOA case of zero degrees two conditions were obtained from AP02, one near the nose tip and one towards the mid to aft section of the airframe. The region between, denoted as the transitional region, is an average of the two conditions. For the ten degree re-entry AOA case a value was obtained from AP02 for each of the three regions.

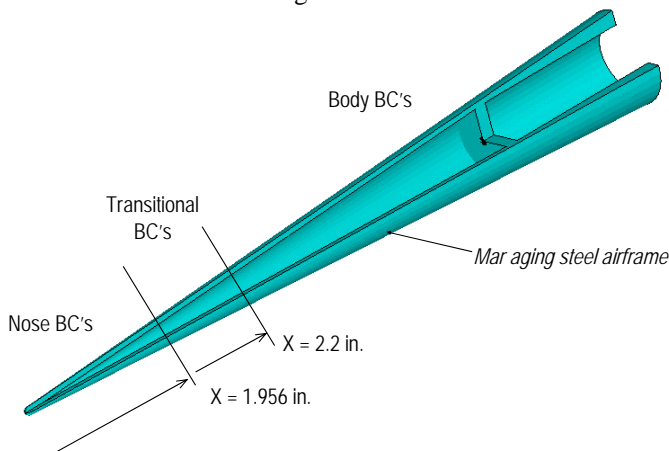


FIGURE 1. AIRFRAME ONLY

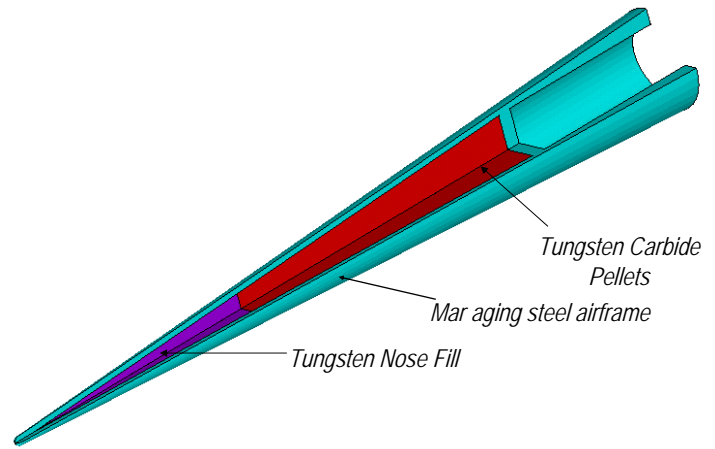


FIGURE 2. AIRFRAME WITH FILL AND PAYLOAD

The boundary condition obtained from AP02 was for a single point on the skin along the centerline at an approximate mean longitudinal coordinate. This condition, although taken from only one point, was applied to all the surface nodes of the region, i.e. nose region, transitional region, or body region. At the present time this analysis is meant to be a first step in numerous iterations. Further refinement of the boundary conditions is necessary in subsequent analyses.

Results

Along the projectile various nodes were selected, approximately mid-thickness, to track the temperature time-history. In the airframe only case three nodes were selected, Node_1, Node_2, and Node_3 as seen in Figure 3; similarly the same three nodes were tracked in the full airframe, tungsten nose fill, and pellet configuration as well as a center node in the nose fill and a center node in the payload.

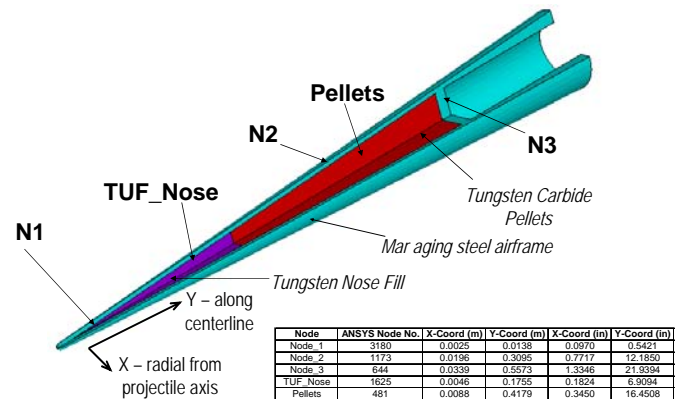


FIGURE 3. PROJECTILE NODE SELECTION

Before looking at the results, it must be made clear that the only difference between the angle of attack case of zero degrees and the angle of attack case of 10 degrees is the re-entry portion of the flight profile. Both flights are assumed to travel at zero degree angle of attack until they reach an altitude of

approximately 125,000 feet. Therefore it is safe to assume that both profiles are identical until the re-entry portion.

This same argument does not apply to the comparison of the two configurations however. With the more detailed model there is an additional thermal mass which helps alleviate some of the maximum temperatures by its thermal capacitance. The maximum temperatures experienced will be slightly different but the trends will be the same.

Constant 0-degree Re-entry Angle of Attack

Airframe Configuration Only. For the airframe only configuration, trends of the thermal time-history can be established. Due to the lack of interior detail – i.e. tungsten nose fill, payload – all of the heat must be distributed throughout the airframe which is the worst case scenario. Figure 4 and Figure 5 show the airframe only temperature time histories.

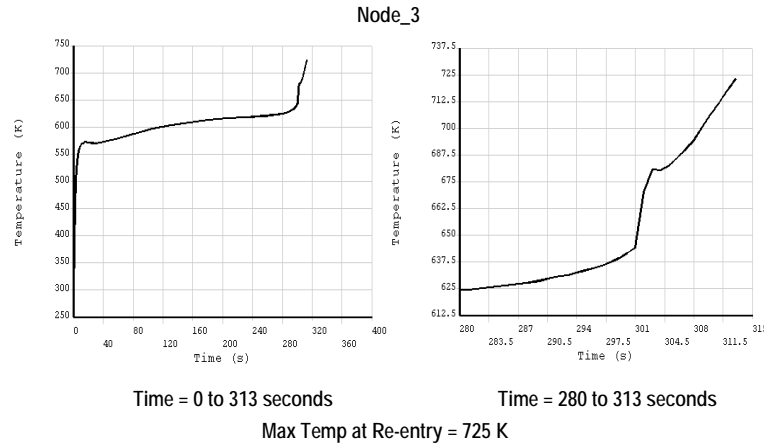


FIGURE 5. AIRFRAME ONLY TEMPERATURE TIME HISTORIES (NODE 3)

As seen in Figure 4 the maximum temperature experienced at Node_1 occurs within the first few seconds of flight. At launch the heat loads experienced by the projectile are the greatest due to the extremely high velocities and low altitudes. It takes approximately three seconds for the maximum heat loads to soak into the airframe such that the temperatures are felt at Node_1.

At Node_1 there is a maximum temperature of 1450 K (2150 °F); maraging steel is approaching its melt temperature (1673 K). More of a concern is that this node is representative of the region. The maximum temperature encountered will be along the surface, particularly at the stagnation point. As a general rule, the skin temperature will be approximately 0.5 – 0.6 times the adiabatic wall temperature – theoretical maximum wall temperature assuming no heat transfer occurs at the surface. With this in mind, the adiabatic wall temperature near the nose is approximately 2600 K. Sixty percent of this temperature is 1560 K, which again is pushing the limits of maraging steel.

At Node_2 and Node_3 the maximum temperatures experienced do not occur until the descent portion of the flight; more precisely at strike. The temperatures in the mid-body and aft sections of the body are highly tied to the heat flux on the nose region and the thermal conductivity. A majority of the heat that enters the body penetrates at the nose region. The rate at which this heat load is distributed through the airframe is directly related to the thermal conductivity of the material, hence the time lag between the maximum heat rates and the maximum temperatures at nodes two and three.

Airframe/Tungsten Nose/Payload Configuration. The initial analysis was further refined by introducing more detail to the model. Instead of the airframe only, representative masses were included for both the solid tungsten nose and the tungsten carbide payload. By increasing the mass of the system - and therefore the thermal capacitance - it would be expected that the overall temperatures be slightly lower in the regions influenced by the additional masses. (Figure 6 and Figure 7).

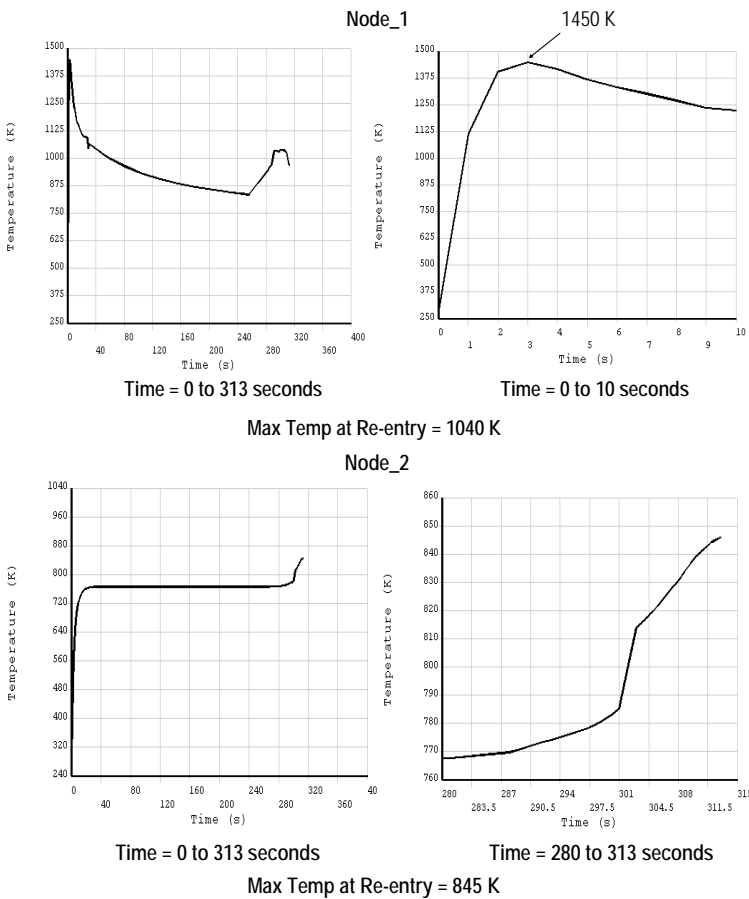


FIGURE 4. AIRFRAME ONLY TEMPERATURE TIME HISTORIES (NODES 1 AND 2)

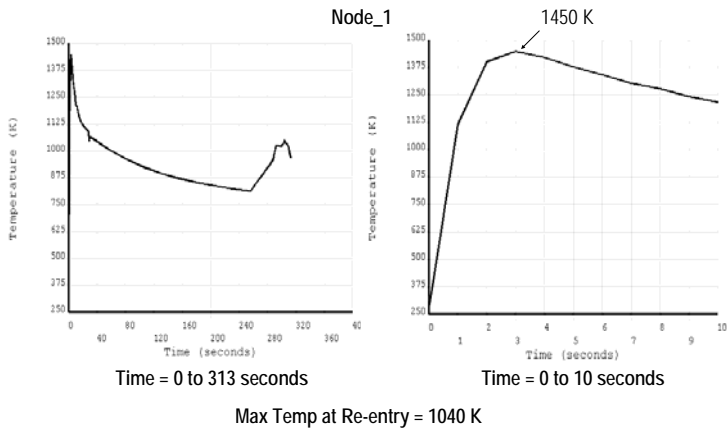


FIGURE 6. AIRFRAME/NOSE FILL/PAYLOAD TEMPERATURE TIME HISTORIES (NODE 1)

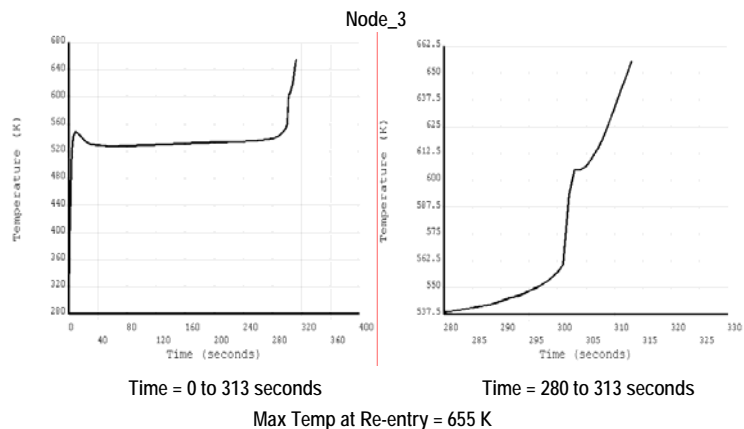
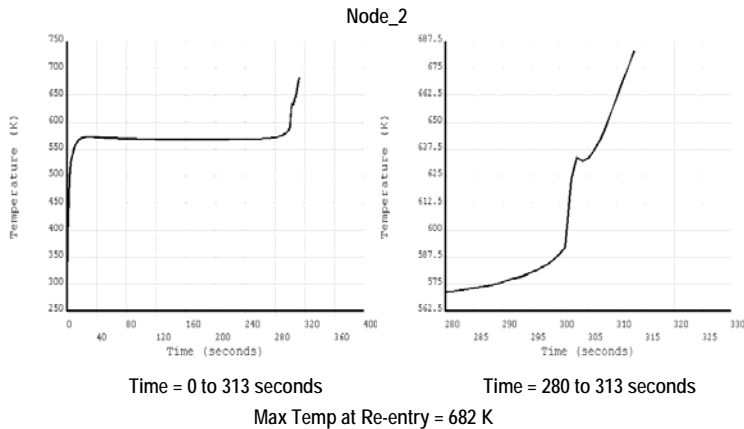


FIGURE 7. AIRFRAME/NOSE FILL/PAYLOAD TEMPERATURE TIME HISTORIES (NODES 2 AND 3)

For Node_1, there was no noticeable change. This is because the additional mass that was added to the system is located well back from the nose region. In essence no change occurred near the nose that would influence the rate at which the wall temperature increases. However, Node_2 and Node_3 both experienced noticeable differences in the maximum temperature achieved: Node_2 (845 K to 682 K) and Node_3 (725 K to 655 K). With the increase in thermal capacitance the system was able

to distribute the heat load over a larger amount of mass than in the airframe only case, therefore reducing the maximum temperature experienced in the middle to aft regions.

Constant 10-Degree Re-entry Angle of Attack. With the increased angle of attack upon re-entry the heat transfer coefficients are increased just rearward of the nose tip. This change in thermal loading slightly increases the maximum temperatures experienced during the re-entry phase of the flight.

Figure 8 shows the results for all cases – both configurations and two re-entry cases. At the nose region, Node_1, there is only a change in the maximum re-entry temperature and not in the maximum temperature experienced overall. For the nose region the most significant heating occurs immediately at launch, highest speed and greatest air density. Since both cases have an angle of attack of zero at launch both results are the same.

Further back on the body is where the angle of attack change impacts the results more significantly. Both configurations experience an increase of about 50 to 75 degrees Kelvin between the zero degree re-entry angle of attack case and the ten-degree re-entry angle of attack. Since the angle of attack shifts the stagnation point rearward, the heat path is slightly shortened to the mid- and afterbody. Node_1 is less influenced by the AOA effects than Node_2, Node_3, and the interior components. Considering 50 to 75 degrees is well within the accuracy of the codes these numbers should be representative of the trends rather than specific results.

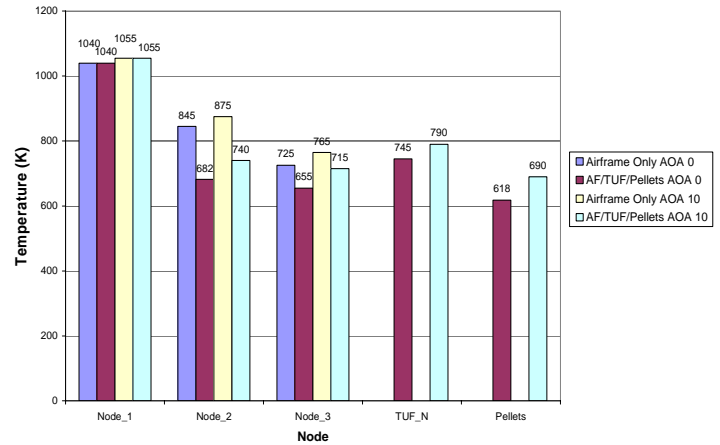


FIGURE 8. ANGLE OF ATTACK INFLUENCE ON RE-ENTRY TEMPERATURE

Conclusions and Recommendations for Future Work

Barring any major performance degradation due to the elevated temperatures, it is safe to say that standard materials can be used for a majority of the airframe components other than regions near stagnation points, such as the nose tip and fin leading edges. These areas will have to be carefully analyzed in future iterations to design appropriate thermal protection systems (TPS).

Temperatures upwards of 700 K (800 °F) are expected in the aft section of the projectile in the region where the electronics canister is intended. Caution must be taken in the design of this

region due to these temperatures which are extreme for electronics. With an appropriate TPS on the nose tip and fin leading edges some of the heat flux into the airframe will be mitigated. Thermal barrier concepts can be employed in this region as well to protect the electronics.

To reiterate, the boundary conditions obtained for this analysis are still at a rudimentary level. Many basic assumptions were made as well as the use of semi-empirical codes. It is highly recommended that the boundary conditions be further refined by making use of higher fidelity aerodynamic and thermal analysis codes in conjunction with the appropriate temperature dependent properties.

ACKNOWLEDGMENTS

The author gratefully acknowledges the Office of Naval Research and PMS405 for funding this effort.

REFERENCES

1. Ellis R.L, Poyner J.C & McGlasson ' Influence of Bore and Rail Geometry on an Electromagnetic Naval Railgun System', IEEE Transactions on Magnetics, Vol. 41, January 2005.
2. Hypersonic and High Temperature Gas Dynamics, Anderson, J.D. McGraw-Hill, 1989.
3. Aeroprediction Code 2002, Aeroprediction Inc., Moore, F.G.
4. Approximate Methods For Weapon Aerodynamics, Moore, F.G. AIAA 2000
5. Eckert, E.R.G. "Engineering Relations for Heat Transfer and Friction in High-Velocity Laminar and Turbulent Boundary Layer Flow over Surfaces with Constant Pressure and Temperature, " Transcript of the American Society of Mechanical Engineers, Vol. 78, No. 6, 1956.
6. Hypersonic Aerothermodynamics, Bertin, J. AIAA 1994
7. ANSYS 8.1 Documentation.